ChemPubSoc Europe
DOI: 10.1002/cphc.201402506
CHEMPHYSCHEM Articles

Deuterium MAS NMR Studies of Dynamics on Multiple Timescales: Histidine and Oxalic Acid**

Monique Chan-Huot,[a, b, c, d, e] Stephen Wimperis,[f] Christel Gervais,[g] Geoffrey Bodenhausen,[a, b, c, h] and Luminita Duma*[a, b, c]

Deuterium (^{2}H) magic-angle spinning (MAS) nuclear magnetic resonance is applied to monitor the dynamics of the exchanging labile deuterons of polycrystalline L-histidine hydrochloride monohydrate-d_7 and α-oxalic acid dihydrate-d_6. Direct experimental evidence of fast dynamics is obtained from T_{1Z} and T_{1Q} measurements. Further motional information is extracted from two-dimensional single-quantum (SQ) and double-quantum (DQ) MAS spectra. Differences between the SQ and DQ linewidths clearly indicate the presence of motions on intermediate timescales for the carboxylic moiety and the D_2O in α-oxalic acid dihydrate, and for the amine group and the D_2O in L-histidine hydrochloride monohydrate. Comparison of the relaxation rate constants of Zeeman and quadrupolar order with the relaxation rate constants of the DQ coherences suggests the co-existence of fast and slow motional processes.

1. Introduction

The spin $I=1$ deuterium (^{2}H) nucleus has been one of the most widely exploited quadrupolar nuclei in solid-state nuclear magnetic resonance (NMR) studies of molecular order and dynamics. The ^{2}H quadrupole interaction dominates the lineshape and is very sensitive to a large range of reorientational motions in solids. This spin $I=1$ nucleus has a moderate quadrupole coupling strength, ranging from 150 to 250 kHz in organic compounds. Therefore, the ^{2}H quadrupole interaction needs to be considered only to first order with respect to the Zeeman interaction. Given that the quadrupole interaction is usually much larger than the range of isotropic ^{2}H chemical shifts in organic compounds, extensively overlapping static spectra are obtained for samples with different chemical sites. ^{2}H line narrowing is observed under magic-angle spinning (MAS) and the first-order quadrupolar interaction leads to a set of narrow sidebands for each isotropic chemical shift.

Early ^{2}H NMR studies of dynamics focused on liquid crystals and/or small molecules dissolved in liquid crystals,[1] plastic crystals,[2] polymers,[3] or protein membranes.[4] ^{2}H NMR spectroscopy is also suitable for characterising dynamics of powdered or crystalline samples. A variety of ^{2}H NMR experiments can provide access to an extraordinarily wide kinetic window. Most solid-state NMR studies of molecular dynamics rely on the analysis of powder patterns by comparing the experimental lineshapes with those simulated for specific models of motional averaging. Furthermore, relaxation parameters can be considered in concert with lineshapes to determine motional timescales. Such studies generally require ^{2}H site-selective isotopic labelling of the system. The effect of molecular motions on spectral parameters such as powder lineshapes depends not only on the type of spin interaction but also on the frequency, amplitude, and orientation of motions. The reorientation of CD_3 groups[5,6] about their C_3 axis has been extensively studied in crystalline amino acids, peptides and proteins. The reorientation of ND_3^+ groups[7] has also been investigated for some crystalline amino acids. Molecular dynamics and local conformational fluctuations are extremely important because they affect the properties of solid materials. Investigating motions such as 180° flips of water molecules can provide essen-

[a] Dr. M. Chan-Huot, Prof. G. Bodenhausen, Dr. L. Duma
Laboratoire des BioMolécules, UMR 7203
UPMC/ENS/CNRS, 24, rue Lhomond,
75231 Paris Cedex 05 (France)
E-mail: luminita.duma@ens.fr
[b] Dr. M. Chan-Huot, Prof. G. Bodenhausen, Dr. L. Duma
Sorbonne Universités, UPMC Univ Paris 06, LBM
4 place Jussieu, 75005, Paris (France)
[c] Dr. M. Chan-Huot, Prof. G. Bodenhausen, Dr. L. Duma
École Normale Supérieure—PSL Research University
Département de Chimie, 24, rue Lhomond
75005 Paris (France)
[d] Dr. M. Chan-Huot
Institut Curie, 91405 Orsay (France)
[e] Dr. M. Chan-Huot
INSERM U759, 91405 Orsay (France)
[f] Prof. S. Wimperis
School of Chemistry and WestCHEM
University of Glasgow
Glasgow G12 8QQ (United Kingdom)
[g] Prof. C. Gervais
Sorbonne Universités, UPMC Univ. Paris 06, CNRS
Collège de France UMR 7574
Chimie de la Matière Condensée de Paris
75005, Paris (France)
[h] Prof. G. Bodenhausen
Institut des Sciences et Ingénierie Chimiques
Ecole Polytechnique Fédérale de Lausanne (EPFL)
Batochime (BCH), 1015 Lausanne (Switzerland)

[**] MAS NMR: Magic-Angle Spinning Nuclear Magnetic Resonance

Supporting Information for this article is available on the WWW under http://dx.doi.org/10.1002/cphc.201402506.

tial insight into the chemical and physical properties of a material.

^{2}H MAS NMR leads to an increase in both sensitivity and resolution because the coherent averaging induced by mechanical rotation of the sample reduces the static spectrum to a manifold of spinning sidebands. The achievable spinning rates are generally smaller than the width of the static quadrupole-broadened powder pattern, so that a set of spinning sidebands remains in the ^{2}H MAS spectra. In the presence of molecular motions, the envelope of the spinning sidebands shows distinctive features that can often be analysed to characterise dynamic processes in detail.[8] Under MAS, resolution can be further improved by exploiting double-quantum (DQ) coherences in two-dimensional experiments. Combined with MAS, this leads to a DQ ^{2}H spectrum in one dimension and a single-quantum (SQ) dimension revealing spinning sidebands that are characteristic of quadrupole effects. However, with few exceptions,[9–14] most ^{2}H NMR studies of dynamics have been carried out on static samples that require site-selective labelling.

In their pioneering work, Maricq and Waugh[15] pointed out that random fluctuations of the orientation of an interaction tensor that lead to distortions of powder patterns in nonrotating samples tend to be even more prominent in spinning samples because they can affect trains of rotational echoes. The coherent rotation of the sample may interfere with these random fluctuations when they occur on the same timescale, which may complicate the interpretation of the dynamics considerably.

^{2}H NMR relaxation is a powerful probe of motional processes in the solid state because the relaxation parameters can often be directly interpreted in terms of rotational and librational motions of molecular fragments. The quadrupolar mechanism is generally dominant. It only depends on the interaction of a single deuteron with the electric field gradient arising from its surroundings. In contrast to proton relaxation in solids, which is usually dominated by ^{1}H–^{1}H dipole-dipole "flip-flop" terms, deuteron spin-lattice relaxation is barely affected by spin diffusion, except in systems for which the ^{2}H sites have only small isotropic chemical shift differences.[16]

In this work, we characterise the dynamics of all labile deuterium sites in L-histidine hydrochloride monohydrate and α-oxalic acid dihydrate, both recrystallised from heavy water, by using a combination of ^{2}H MAS SQ–DQ correlation spectra and T_{1Z}, T_{1Q} relaxation measurements as a function of temperature. In studies in the liquid state, in which fast motions are dominant, measurements of five ^{2}H spin-spin and spin-lattice relaxation rate constants in the side-chains[17] and backbone[18] of proteins have been shown to achieve internal consistency. Even though the direct applicability to solids remains to be proven, we have attempted to apply this approach to our data. An analysis of the parameters reflecting the timescales of the different deuterium sites shows discrepancies between the DQ relaxation rates measured experimentally and the relaxation rates calculated in the fast motion limit of the Redfield approximation. The T_{1Z} and T_{1Q} relaxation measurements probe fast motions; therefore, we believe that the difference between the experimental and calculated DQ relaxation rate constants allows us to make an approximate separation of fast and slow motions contributing to the widths of the DQ transitions.

Materials and Methods

Sample Preparation

Crystalline L-histidine hydrochloride monohydrate-d_7 and α-oxalic acid dihydrate-d_6 (see Figure 1) were dissolved in ^2H_2O (Eurisotop, 99% deuteration) at room temperature. Recrystallisation was conducted in a dessicator to avoid absorbing light water from the atmosphere. Adding silica gel accelerated crystallisation. After two days, the dry crystals had grown to a fine powder and were transferred to a 4 mm rotor (ZrO_2). Recrystallisation with ^2H_2O led to the replacement of exchangeable protons by deuterons in L-histidine and α-oxalic acid, including those of the carboxylic and amine groups. Samples were stored at room temperature in an airtight box to avoid exchange with atmospheric water. For both compounds, atomic coordinates obtained from the Cambridge Structural Database (CSD) were used to determine the internuclear distances. For L-histidine hydrochloride monohydrate, only a neutron diffraction structure of the protonated sample[19] has been published (CSD reference code HISTCM12). On the other hand, for the α polymorph of oxalic acid dihydrate, neutron diffraction structures for both protonated[20] and deuterated[21] compounds have been determined. Their corresponding CSD reference codes are OXACDH06 and OXACDH33, respectively.

NMR Spectroscopy

NMR measurements were performed with a 400 MHz (^{2}H Larmor frequency 61.4 MHz) widebore Bruker spectrometer equipped with a 4 mm triple-resonance probe. For all experiments, the temperature was set between 248 and 358 K in steps of 10 K using gas flows of 935 or 2000 L h^{-1}. In all cases, the temperature corresponds to the regulated temperature indicated by the thermocouple. The samples were spinning at 10 kHz, which corresponds to a rotor period of $\tau_{rot} = 100$ μs. The samples were cooled or heated to the desired temperature and allowed to stabilise for at least 30 min under rotation. In all experiments, π/2 radiofrequency excitation pulses of 2.7 μs were used. To obtain fully relaxed spectra, recovery intervals of 2.5 s (at 248 and 258 K) or of 1 s (for all other temperatures) have been used. The ^{2}H Zeeman spin-lattice relaxation times (T_{1Z}) were measured with an inversion-recovery sequence (see Figure 2a), for which the Zeeman magnetization was inverted with a π pulse. After a variable recovery interval τ, which has been incremented from 100 μs to 2.5 s (18 values), a simple π/2 excitation pulse was applied to monitor the ^{2}H magnetization. The integral of each ^{2}H resonance obtained after deconvolution based on a Lorentzian function was calculated. The signal recovery was fitted as a function of τ by using a single exponential function: $M_z(\tau) = M_0(1 - A\exp(-\tau/T_{1Z}))$, where A and T_{1Z} are adjustable parameters (the coefficient A was close to 2). A broadband version of the Jeener–Broekaert sequence[22–24] was implemented under MAS (see Figure 2b) for measuring the ^{2}H quadrupolar-order relaxation times T_{1Q}. The interval $\tau_1 = 0.5$ μs was optimised experimentally. The time-dependence of the area under each ^{2}H resonance, after deconvolution based on a Lorentzian function, was fitted by using a single exponential function: $M_z(\tau) = M_0\exp(-\tau/T_{1Q})$, where T_{1Q} was the only adjustable parameter. Two-dimensional ^{2}H–^{2}H SQ–DQ MAS spectra were recorded with the pulse sequence shown in Figure 2c. Double-quantum coherences are excited by the first pair of π/2 pulses and reconverted into longitudinal magnetization by the

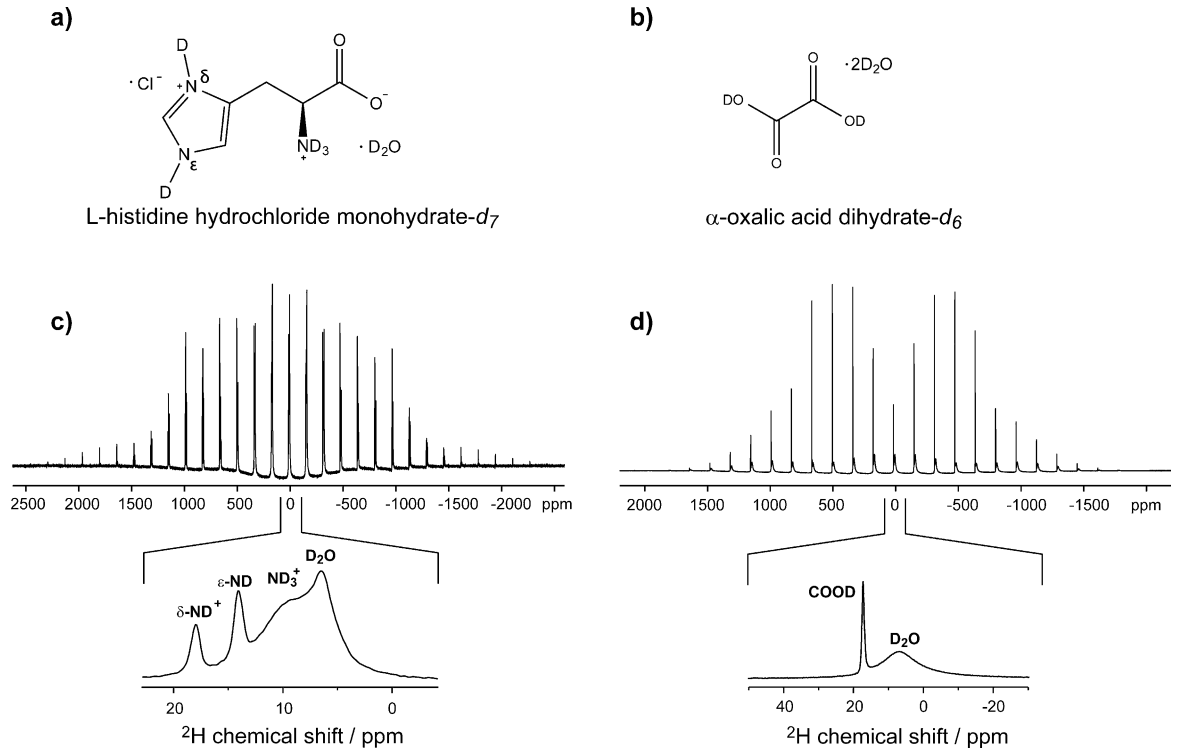

Figure 1. L-Histidine hydrochloride monohydrate-d_7 (a) and α-oxalic acid dihydrate-d_6 (b). ^{2}H MAS spectra recorded with a 9.4 T magnet at 10 kHz spinning frequency and 298 K are shown for L-histidine (c) and oxalic acid (d). The centre band region is shown expanded below each ^{2}H MAS spectrum with the corresponding assignment.

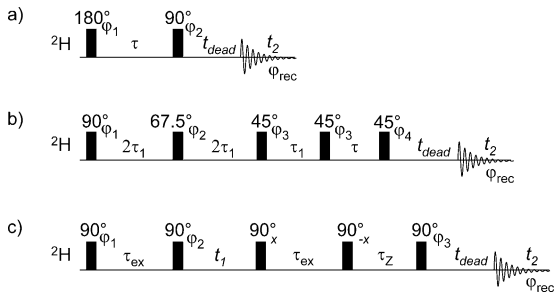

Figure 2. Pulse sequences used for recording ^{2}H Zeeman spin-lattice relaxation times T_{1Z} (a), ^{2}H quadrupolar relaxation times T_{1Q} (b) and ^{2}H–^{2}H SQ–DQ correlation (c) experiments under magic-angle spinning. ^{2}H T_{1Z} relaxation has been measured with the inversion-recovery pulse scheme (a) using the following phase cycle: φ_1=x, −x; φ_2=x, x, −x, −x, y, y, −y, −y; φ_{rec}=φ_2. The broadband Jeener–Broekaert pulse sequence[22–24] (b) has been used for the measurement of ^{2}H T_{1Q} relaxation. The $2\tau_1$ delay was experimentally optimised to 1 μs and the phase cycle was the following: φ_1=8*{x}, 8*{−x}, 8*{y}, 8*{−y}; φ_2=4*{−y}, 4*{y}, 4*{y}, 4*{−y}, 4*{x}, 4*{−x}, 4*{−x}, 4*{x}; φ_3=4*{y}, 4*{−y}, 4*{−y}, 4*{y}, 4*{−x}, 4*{x}, 4*{x}, 4*{−x}; φ_4=4*{−x, −y, x, y, x, y, −x, −y}; φ_{rec}=8*{−x, −y, x, y}. The ^{2}H–^{2}H SQ–DQ MAS (c) experiment[48,49] used the following phase cycle: φ_1=x, y, −x, −y; φ_2=−x, −y, x, y; φ_3=4*{x}, 4*{y}, 4*{−x}, 4*{−y}; φ_{rec}=x, −x, x, −x, y, −y, y, −y, −x, x, −x, x, −y, y, −y, y. The delays for the excitation of double-quantum coherence and the z-filter were 3 and 2 μs, respectively. We used the States method to obtain pure-absorption two-dimensional lineshapes by means of a hypercomplex Fourier transform. The dead-time prior to acquisition was set to 30 μs for all pulse sequences, entailing a frequency-dependent phase correction. The relaxation delays for the T_{1Z} and T_{1Q} experiments are indicated in the experimental section.

second pair of π/2 pulses. The t_1 interval was synchronised with the rotor period giving a spectral width of 10 kHz in the indirect dimension. Free induction decays comprising 16384 t_2 points were collected for each of 256 t_1 points. The intervals for the excitation of the double-quantum coherence and the z-filter were 3 and 2 μs, respectively. The z-filter leads to relatively clean in-phase spectra. The dead-time prior to acquisition was set to 30 μs for all pulse sequences. The phase cycling used for each of the three pulse schemes is given in the legend of Figure 2. The magic angle was directly adjusted by minimising the ^{2}H linewidth of the δ-ND$^+$ resonance in L-histidine hydrochloride monohydrate and of the COOD resonance in α-oxalic acid dihydrate, respectively.

Data Analysis

All raw experimental data were processed by using the TopSpin program (Bruker) and further analysed with a home-written program based on Mathematica 8. This program was developed for the deconvolution of the different ^{2}H sites for each spinning sideband and to analyse the relaxation times T_{1Z} and T_{1Q} by using a global fitting approach. The Arrhenius-type studies of the relaxation rates and of the SQ and DQ linewidths have also been performed with a home-written Mathematica program. All programs are available upon request.

Error Estimates

The stochastic errors in the T_{1Z}, T_{1Q} experiments obtained from repeat measurements at the same temperature were less than 0.2%. Systematic errors arising from radiofrequency miscalibration and/or inhomogeneity, magic-angle mis-set, small temperature var-

iations, and small spinning instabilities are expected to have significant and different contributions to the individual spinning sideband manifolds. At 10 kHz spinning frequency, the anisotropy of T_{1Z} and T_{1Q} relaxation times is expected to be small in solids. The T_{1Z} and T_{1Q} values were averaged over all spinning sidebands, except the centre band, which has been excluded from T_{1Q}. The error bars correspond to the standard deviation.

First-Principles Calculations

First-principles calculations based on the gauge-including projector-augmented wave (GIPAW) method[25] were performed within Kohn–Sham DFT using the QUANTUM-ESPRESSO code.[26] The crystalline structure is described as an infinite periodic system using periodic boundary conditions. The NMR calculations were performed for the experimental geometries determined by diffraction for both L-histidine hydrochloride monohydrate[19] and deuterated α-oxalic acid dihydrate.[21] For both samples, the experimental structures have been used. The Perdew–Burke–Ernzerhof (PBE) generalised gradient approximation[27] was used and the valence electrons were described by norm-conserving pseudopotentials[28] in the Kleinman–Bylander[29] form. The wavefunctions are expanded on a plane wave basis set with a kinetic energy cut-off of 80 Ry. The principal components V_{xx}, V_{yy}, and V_{zz} of the electric field gradient (EFG) tensor, with the convention $|V_{zz}| \geq |V_{xx}| \geq |V_{yy}|$, were obtained by diagonalisation of the tensor. The quadrupolar interaction can then be characterised by the quadrupolar coupling constant C_Q and by the asymmetry parameter η, which are defined as $C_Q = eQV_{zz}/h$ and $\eta = (V_{yy} - V_{xx})/V_{zz}$. The nuclear quadrupole moment reported by Pyykko[30] for ^2H ($Q = 2.86$ mb) was used in these calculations.

2. Theoretical Background

The ^2H NMR relaxation rates are mainly determined by the interaction between the quadrupolar moment of the deuteron and the electric field gradient (EFG) at the ^2H nucleus in each molecular site. The EFG tensor is extremely sensitive to averaging by molecular motions, and this effect is not only revealed by spectral lineshapes but also by relaxation times. In all cases, appropriate theoretical models relating the various measured quantities to the relevant parameters describing the dynamic processes are required to extract dynamic information.

The ^2H relaxation rates of the Zeeman order (i.e. $<I_z>$) and the quadrupolar order (i.e. $<3I_z^2 - 2E>$) are sensitive to fast motions, which are well approximated by Redfield theory.[31] T_{1Z} and T_{1Q} are referred to as the Zeeman and quadrupolar relaxation times and they describe the return to equilibrium of Zeeman magnetization and the decay of quadrupolar order. In the fast-motion limit (Redfield), Equations (1a), (1b), (1c), and (1d) can be derived for the longitudinal, single- and double-quantum relaxation rate constants,[17,32,33] considering the general case of an asymmetric EFG tensor:

$$R_{1Z} = \frac{1}{T_{1Z}} = \frac{3C_Q^2}{40}\left(1 + \frac{\eta^2}{3}\right)[J_1(\omega_0) + 4J_2(2\omega_0)] \quad (1a)$$

$$R_{1Q} = \frac{1}{T_{1Q}} = \frac{3C_Q^2}{40}\left(1 + \frac{\eta^2}{3}\right)[3J_1(\omega_0)] \quad (1b)$$

$$R_{SQ} = \frac{3C_Q^2}{40}\left(1 + \frac{\eta^2}{3}\right)[3J_0(0) + 5J_1(\omega_0) + 2J_2(2\omega_0)] \quad (1c)$$

$$R_{DQ} = \frac{3C_Q^2}{40}\left(1 + \frac{\eta^2}{3}\right)[J_1(\omega_0) + 2J_2(2\omega_0)] \quad (1d)$$

We note that motions at the Larmor frequency and twice this frequency dominate the relaxation of Zeeman order and double-quantum coherences, whereas motions at the Larmor frequency govern the relaxation of quadrupolar order. Single-quantum coherences are affected by motions at frequencies 0, ω_0 and $2\omega_0$. The dependence of R_{SQ} on $J_0(0)$ renders the SQ linewidths sensitive to slow motional processes.

3. Results and Discussion

3.1. ^2H MAS Spectra and ^2H Tensor Parameters

The magnitude of the quadrupolar coupling constants of deuterons in rigid environments varies between approximately 150 and 250 kHz. In the presence of motion, the reorientation of the ^2H quadrupole tensor will produce a jump in the precession frequencies of the SQ coherences during a rotor period and this will interfere with the formation of the rotational echoes at the end of each rotor period.

Figure 3 displays the intensity of the centre band and spinning sidebands obtained by deconvolution of ^2H MAS single-pulse spectra at 298 K with a Lorentzian resonance profile for each individual ^2H site in: a) L-histidine hydrochloride monohydrate and b) α-oxalic acid dihydrate. Centre band and spinning sidebands have been fitted independently with their own model linewidths. The deconvolution was performed with a home-written Mathematica program and the signal was normalised with respect to the most intense signal for each compound (i.e. ND_3^+ for L-histidine and COOD for α-oxalic acid). The shape of the envelope of the spinning sidebands thus obtained is preserved throughout the full temperature range exploited in this work. The spinning sideband envelope has also been analysed with the SOLA routine of the TopSpin program (Bruker) to extract the quadrupolar tensor parameters for each deuterium site as a function of temperature; the tensor parameters thus obtained are tabulated in the Supporting Information, SI. In principle, the spinning sideband patterns contain the complete information on the anisotropy and asymmetry of the quadrupolar interaction. In an exhaustive study comparing the reliability of the determination of tensor parameters in solid-state NMR experiments under static and spinning conditions,[34] the best spinning frequency for the accurate determination of the quadrupolar interaction has been found to be near $\nu_{rot}/C_Q = 0.25$, for $0.2 < \eta < 0.75$. If the asymmetry parameter is $0.25 < \eta < 0.55$, it can be most accurately estimated from MAS spectra if $\nu_{rot}/C_Q \approx 0.15$. However, for $\eta = 0$ or 1, static spectra are always more reliable. Our results obtained by fitting sideband patterns are in good agreement with quadrupolar tensor parameters obtained by different measurements.[35,36] Indeed, except for ND_3^+, which has a ν_{rot}/C_Q ratio of approximately 0.2, the size of the quadrupolar interaction of all other

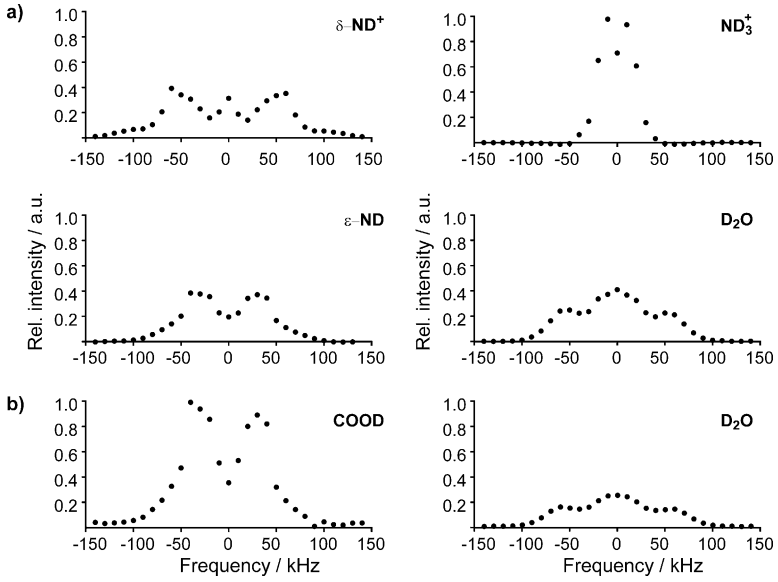

Figure 3. Deconvolution of ^{2}H MAS single-pulse spectra at 298 K with a Lorentzian resonance profile for each individual ^{2}H site in L-histidine hydrochloride monohydrate (a) and α-oxalic acid dihydrate (b). Only the intensities of the centre band and spinning sidebands are given. Their amplitudes were normalised with respect to the highest signal for each compound (i.e. ND_3^+ for L-histidine hydrochloride monohydrate and COOD for α-oxalic acid dihydrate). The envelope of the spinning sidebands conserves the same shape over the whole temperature range exploited in this work.

^{2}H sites is large enough so that the regime of slow spinning applies for $\nu_{rot} = 10$ kHz ($\nu_{rot}/C_Q \approx 0.05$), where the quadrupolar tensor parameters can be determined with good accuracy. The quadrupolar coupling constant of both ^{2}H sites in α-oxalic acid dihydrate varies between 4 to 6% over the temperature range of observation, and decreases with decreasing temperature as observed previously by Chiba and Soda[35] on the α and β polymorphs of oxalic acid dihydrate. It has been shown in single crystals that the magnitude of the ^{2}H quadrupole coupling in an O–D···O system depends on the strength of the hydrogen bonding, with a significant decrease of C_Q with increasing hydrogen-bond strength.[37] The C_Q values for ND_3^+ and D_2O motionally averaged sites in L-histidine hydrochloride monohydrate remain almost constant within the error bars for all temperatures, whereas they increase with temperature by approximately 6% for δ-ND^+ and decrease by approximately 9% for ε-ND (see Table S1). Since small changes are observed in the shape manifold, these small temperature variations of the C_Q constants for the different deuterons in oxalic acid and L-histidine may be the result of libration motions and should be used with caution. First-principles Car–Parrinello molecular dynamics simulations were able to reproduce the experimentally observed C_Q value at 305 K for benzoic acid[38] but such calculations are beyond the scope of the present work. Table 1 summarises the quadrupolar coupling constants and asymmetry parameters of all ^{2}H sites extracted from the spinning sideband pattern at 25 °C using the SOLA routine of TopSpin (Bruker). These are compared to those obtained by first-principles calculations starting from the neutron diffraction structures of both compounds and to experimental values obtained in previous works using off-MAS experiments[36] for L-histidine hydrochloride monohydrate and using ^{2}H NMR spectroscopic analysis of single crystals[35] for α-oxalic acid dihydrate. To gain a quantitative interpretation of the quadrupole coupling constant values obtained for δ-ND^+ and ε-ND, Hoffmann and Schnell[36] exploited an empirical relationship between the C_Q (in kHz) and the internuclear distance (in Å) between the donor and the acceptor in a hydrogen bond. This relation was first introduced by Soda and Chiba[39] for O–D···O bonds and further extended by Hunt and MacKay[40,41] to N–D···O, N^+–D···O and N^+–D···Cl^-. However, the linear dependence that Hoffmann and Schnell derived[36] differed from the one originally published,[40,41] which may explain, in addition to the

Table 1. Quadrupolar coupling constants and asymmetry parameters for ^{2}H sites in perdeuterated L-histidine hydrochloride monohydrate and α-oxalic acid dihydrate.

Molecule	Deuterium site	C_Q [kHz]	η
L-histidine hydrochloride monohydrate	δ-ND^+	103 ± 2[a]	0.22 ± 0.05[a]
		120 ± 2[d]	0.1 ± 0.2[d]
		110[e]	0.19[e]
		137[f]	
	ε-ND	156 ± 2[a]	0.12 ± 0.05[a]
		181 ± 2[d]	0.1 ± 0.2[d]
		196[e]	0.1[e]
		174.8[f]	
	ND_3^+[c]	39 ± 2[a]	0 ± 0.05[a]
		50 ± 2[d]	0 ± 0.2[d]
		169[e]	0.03[e]
		48.2[f]	
	D_2O[c]	98 ± 2[a]	0.85 ± 0.05[a]
		118 ± 2[d]	0.9 ± 0.2[d]
		259[e]	0.13[e]
		110.4[f]	
α-oxalic acid dihydrate	COOD	118.0 ± 1.1[b]	0.11 ± 0.01[b]
		115 ± 2[d]	0.1 ± 0.2[d]
		106[e]	0.12[e]
		137.1[f]	
	D_2O[c]	125.6 ± 1.3[b]	0.89 ± 0.02[b]
		122 ± 2[d]	0.9 ± 0.2[d]
		275[e]	0.11[e]
		122.2[f]	

[a] Measured by off-MAS experiments (0.71°) at $\nu_{rot} = 29.762$ kHz[36] without temperature regulation. [b] From deuteron magnetic resonance on a single crystal[35] at 298 K. [c] Motionally averaged. [d] This work, from spinning sideband analysis with SOLA routine from TopSpin (Bruker) at $\nu_{rot} = 10$ kHz and 25 °C. [e] First-principles calculations. The values given for ND_3^+ and D_2O sites correspond to averages over the tensor parameters of different sites. [f] Using the following equations: $C_Q = 328 - 643/r(D\cdots O)^3$ for O–D···O, $C_Q = 282 - 572/r(D\cdots O)^3$ for N–D···O, and $C_Q = 253 - 572/r(D\cdots O)^3$ for N^+–D···O with C_Q in kHz and r(D···O) in Å.[39–41]

temperature effects, the deviations they observed between the measured and calculated C_Q values. It should also be noted that different equations [$C_Q = 282 - 572/r(D\cdots O)^3$ for N–D···O and $C_Q = 253 - 572/r(D\cdots O)^3$ for N^+–D···O with C_Q in kHz and r(D···O) in Å] have to be used for the two amides of the imidazole ring because δ-ND^+ is protonated in the zwitterionic form.

The ^{1}H and ^{2}H MAS spectra of perdeuterated L-histidine hydrochloride monohydrate display δ-NH^+ and ε-NH resonances in the high-frequency region at approximately 17 and 13 ppm, respectively (data not shown). It is well established that NMR chemical shifts are very sensitive to the strength of hydrogen bonding, and a ^{1}H chemical shift towards higher frequency is characteristic of a stronger hydrogen bond. Thus, δ-ND^+ seems to be involved in a stronger hydrogen bond than ε-ND due to crystal packing and to mesomeric and inductive effects of surrounding chemical moieties. This agrees well with neutron diffraction,[19] MD calculations[42] and NMR studies,[43–45] which demonstrate the existence of a strong intermolecular hydrogen bond between the hydrogen atom of the δ-NH^+ and the carboxyl oxygen of the neighbouring molecule. NMR results[44] have associated weaker N–H dipolar couplings (i.e. longer internuclear distances) with an altered potential indicative of a strong intermolecular N–H···O hydrogen bond. It has been shown that for strong hydrogen bonds (i.e. for r(N···O) < 2.7 Å) the N–H internuclear distance becomes longer. We expect the same behaviour for the N–D···O hydrogen bond in the perdeuterated sample.[46] Hence, an increase in the N–D internuclear distance if r(N··O) < 2.7 Å will lead to shorter D···O distances and therefore to smaller C_Q values for strong hydrogen bonds, based on the empirical correlation between C_Q and $1/r(D\cdots O)^3$.

Analysis of the one-dimensional ^{2}H MAS spectra (not shown) reveals a decrease in the intensity of the spinning sideband envelope as the temperature is decreased, except for the COOD site in α-oxalic acid dihydrate, which shows the opposite behaviour. Given that the integral remains the same, a broadening of the ^{2}H SQ coherences is observed and confirmed by the SQ–DQ MAS spectra.

3.2. ^{2}H–^{2}H SQ–DQ MAS Spectra

To a first approximation, ^{2}H double-quantum transitions should not exhibit motional broadening because they will be largely unaffected by first-order quadrupolar interactions and hence by molecular motion. SQ–DQ MAS spectra have been previously exploited[47,48] to probe dynamics in solid compounds. Cutajar et al.[48] introduced a simple analytical model to quantify the effects of dynamics on linewidths in ^{2}H SQ MAS NMR spectra. They exploited a spin-echo model based on symmetrical two-site exchange and showed how this can be used to estimate rate constants for the reorientation of the two deuterons when a D_2O molecule flips about its C_2 axis. Hogg et al.[49] used the ratios of the rotary echoes to obtain information about the conformational dynamics of d_8-1,4-dioxane included in the channel solvate hydrate formed with the drug molecule Finasteride. Moreover, Thrippleton et al.[50] compared the spin-echo method with numerical simulations and discussed the agreement of the spin-echo method with earlier linewidth predictions.[15,51] It is worth mentioning that the spin-echo model describes motionally broadened MAS linewidths under all motional regimes, provided the MAS linewidths of the SQ coherences are two to three orders of magnitude greater than those of the DQ coherences. The spin-echo model breaks down when the exchange rate constant k approaches the Larmor frequency ω_0. In this limit, nonsecular terms in the quadrupolar Hamiltonian can no longer be neglected and the dynamics become rapid enough to induce $\Delta m_I = \pm 1$ and ± 2 transitions, which result in the broadening of both SQ *and* DQ transitions by the quadrupolar interaction. The ^{2}H–^{2}H SQ–DQ MAS spectra (see Figure 4a and d) recorded for L-histidine hydrochloride monohydrate and oxalic acid dihydrate show the effect of the reorientation of ND_3^+ and D_2O molecules. Significant motional broadening of SQ coherences is observed for ND_3^+ in L-histidine hydrochloride monohydrate and D_2O in oxalic acid dihydrate at temperatures below 288 K. Only small differences between the SQ and DQ linewidths are observed for D_2O in L-histidine at 248 K. Except ND_3^+ in L-histidine, for which SQ linewidths are greater than the DQ linewidths over the whole temperature range investigated, all other motionally broadened D_2O resonances exhibit broader DQ coherences at high temperature. A rotational motion of the COOD group appears unlikely. Indeed, we observe that the behaviour of COOD stands in contrast with all other deuterium sites by the fact that the DQ linewidths are larger than the SQ linewidths at all temperatures investigated, and that the difference in linewidth increases with temperature. The ratio between DQ and SQ linewidths varies between approximately 2.6 at low temperature to 1.8 at high temperature. DQ coherences that have twice the linewidth of the SQ coherences were observed in deuterated ferrocene-d_{10}.[52] This observation was assigned to the inhomogeneity of the static field and to anisotropic susceptibility, which has an effect that is twice as strong for DQ than for SQ transitions. In our case, inhomogeneous broadening cannot be excluded. However, our results suggest the presence of fast dynamics that leads to simultaneous and perhaps differential broadening of *both* SQ and DQ linewidths.

The temperature dependence of the deuterium linewidths was exploited to estimate the activation barrier of the COOD, ND_3^+ and D_2O groups in the crystalline solid. For water, it has been shown that when the molecule is held in place by hydrogen bonds such as A···D–O–D···B, the reorientational activation energy may be seen as the work required to break these hydrogen bonds.[53] Assuming that this is the only mechanism responsible for motional broadening, the activation barrier provides a measure of the strength of the hydrogen bond.

For a thermally activated dynamic process, the rate constant k can be described empirically by the Arrhenius equation $k = A\exp(-E_a/RT)$. The temperature dependence of the SQ and DQ linewidths allows an Arrhenius-type analysis to be performed for all deuteron sites exhibiting motional dynamics. The results based on Arrhenius-type analysis, considering that the linewidth depends on the inverse of the exchange rate constant, are shown in Figure 5 and summarised in Table 2. In the case

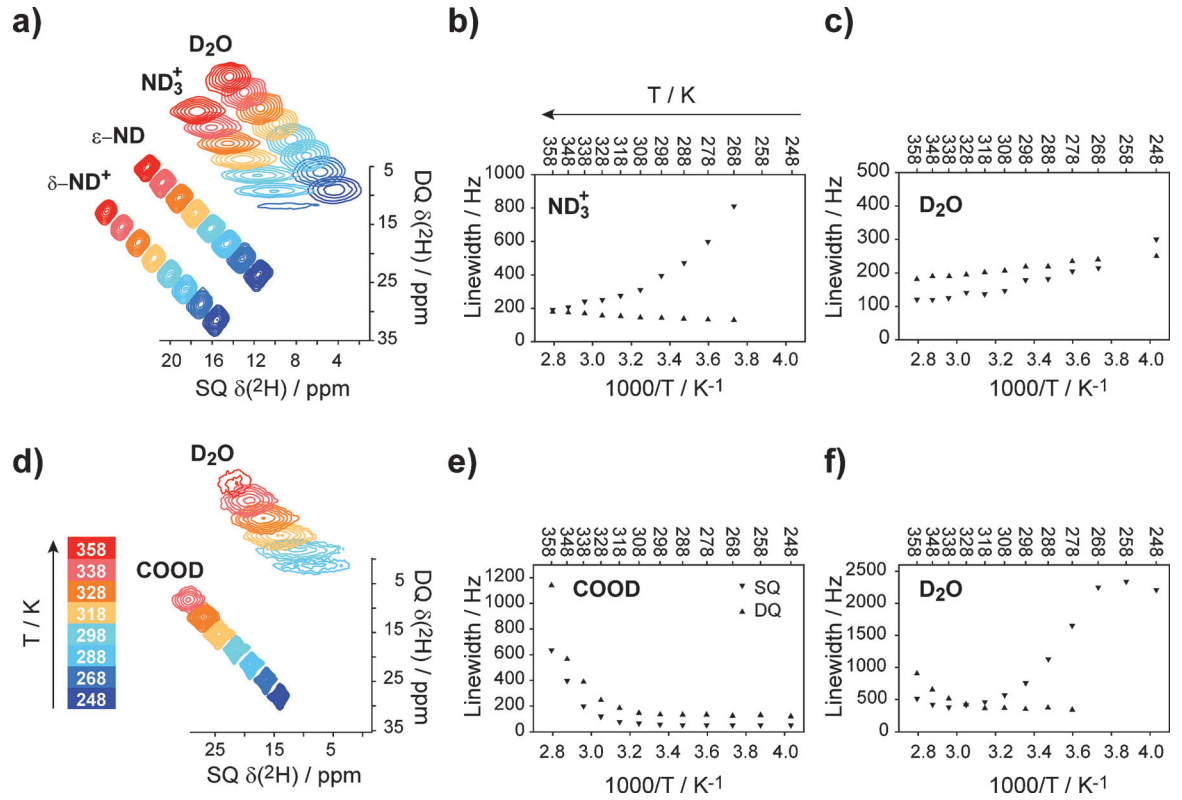

Figure 4. ^{2}H–^{2}H SQ–DQ MAS spectra as a function of temperature for L-histidine hydrochloride monohydrate (a) and α-oxalic acid dihydrate (d). The linewidths at half height of the SQ and DQ coherences versus the inverse of the temperature are shown for ND_3^+ and D_2O in L-histidine hydrochloride monohydrate (b, c) and COOD and D_2O in α-oxalic acid dihydrate (e, f). Only the ^{2}H sites exhibiting motional dynamics are shown.

of L-histidine, the average activation energies of the motional process are negligible for both ND_3^+ and D_2O DQ linewidths, whereas they were estimated to be approximately 14 kJ mol^{-1} for ND_3^+ and approximately 6 kJ mol^{-1} for D_2O SQ linewidths. This suggests that only SQ linewidths are sensitive to motion. These low activation energies are characteristic of small angle, restricted librations. No neutron diffraction structure is known for the perdeuterated L-histidine hydrochloride monohydrate; therefore, we examined the structure of the protonated sample obtained by neutron diffraction at room temperature[19] to rationalise the activation energies for the motion-induced SQ transitions. ND_3^+ is involved in three noncoplanar hydrogen bonds (two N–H···O and one N–H···Cl$^-$) with the internuclear distances r(N···O) = 2.8 Å and r(N···Cl$^-$) =

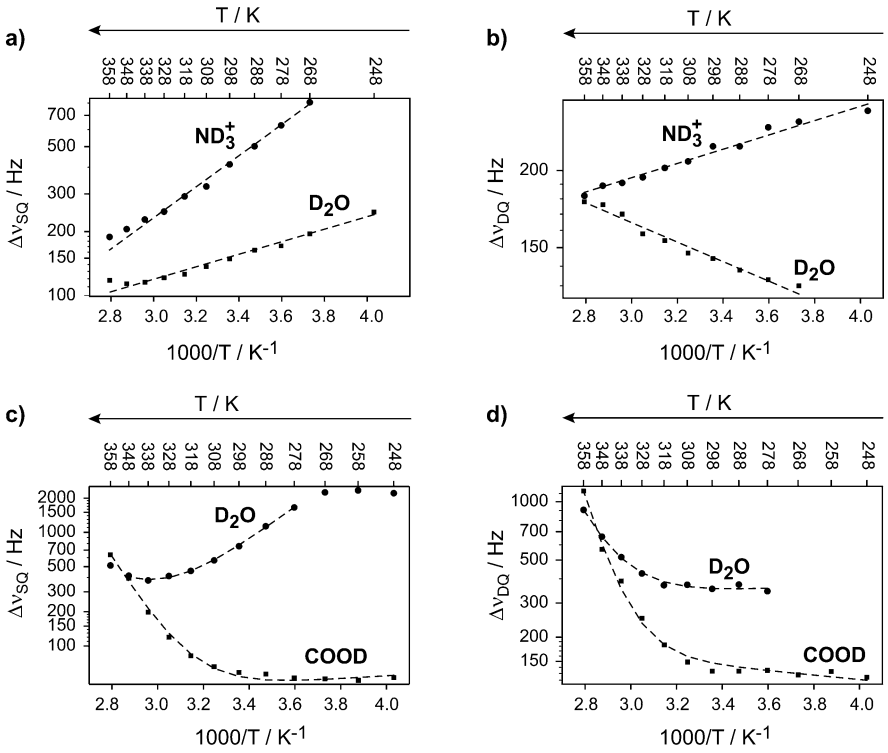

Figure 5. ^{2}H linewidths of SQ (a, c) and DQ (b, d) coherences presented as Arrhenius-type graphs $\Delta\nu$ vs. (1000/T) for L-histidine hydrochloride monohydrate (a, b) and α-oxalic acid dihydrate (c, d), with corresponding fits (dashed lines).

Table 2. Activation energy averaged over all spinning sidebands for individual ^{2}H sites in L-histidine hydrochloride monohydrate and α-oxalic acid dihydrate for SQ and DQ linewidths.

Compound	^{2}H site	E_a (SQ) [kJ mol^{-1}]	E_a (DQ) [kJ mol^{-1}]
L-histidine hydrochloride monohydrate[a]	ND_3^+	13.9 ± 0.5	3.0 ± 0.5
	D_2O	5.6 ± 0.5	2.2 ± 0.5
α-oxalic acid dihydrate	COOD	62.7 ± 0.5	80.8 ± 0.5
	D_2O	28.7 ± 0.5	58.8 ± 0.5

[a] Average E_a cannot be measured for the sites δ-ND^+ and ε-ND.

3.2 Å, both characteristic of weak hydrogen bonds. Instead, the crystal water is involved in three weak hydrogen bonds (two O–H···O and one O–H···Cl^-) with the distances r(O···O) = 3.2 Å and r(O···Cl^-) = 2.8 Å. As the energy required for breaking a hydrogen bond is of the order of 4.5 kcal mol^{-1} (19 kJ mol^{-1}), the estimated activation energies for ND_3^+ and D_2O look plausible because all deuterons in the crystal are involved in weak hydrogen bonds that hinder either the ND_3^+ rotation or the D_2O 180° jumps. Hoffmann[54] also studied the reorientation of the ND_3^+ group by analysing how ^{2}H linewidths in one-dimensional ^{2}H MAS spectra change with temperature at $\nu_{rot} = 15$ kHz and found an activation barrier energy of approximately 30 kJ mol^{-1}, which is more than twice as large as the value we measured by SQ–DQ MAS experiments. At low temperatures, the reorientational averaging of the quadrupole tensor is greatly reduced and the extreme broadening of the ND_3^+ resonances may prevent an accurate estimate of the deuteron linewidths in conventional ^{2}H MAS spectra, as shown by Hoffmann.[54]

The data presented in Figures 5c, d cannot be fitted by postulating a single activation energy over the entire temperature range. The nonlinear Arrhenius behaviour observed for the two deuterium sites in oxalic acid dihydrate indicates the presence of slow motional processes. An orientational order–disorder transition can be ruled out because it would lead to a jump in the relaxation rate constants and not to a plateau. High activation energies have been obtained from the linear slopes of COOD and D_2O resonances in oxalic acid dihydrate, both SQ and DQ motion-induced transitions. Such high activation barriers are characteristic of large-angle jump-type motions. The neutron diffraction structure of deuterated oxalic acid dihydrate[55] contains a short hydrogen bond that connects the carboxylic OH group to crystal water oxygen. The average activation energies derived for COOD and D_2O in oxalic acid indicate that other factors may contribute to the activation barrier in addition to the breaking of hydrogen bonds.

3.3. ^{2}H T_{1Z} and T_{1Q} Measurements

Our samples recrystallised from heavy water may contain some residual protons in the ND_3^+ groups. The ^{1}H–^{2}H dipole–dipole contributions are expected to be small because the R_{1Z} relaxation rate constants are similar (within the error bars) with and without ^{1}H decoupling (data not shown). The ^{14}N–^{2}H dipole–dipole couplings that could be on the order of a few kilohertz should be averaged out by spinning at a frequency of 10 kHz. Owing to the complex orientational dependency of second-order dipolar-quadrupolar cross-terms, second-order effects that are not immediately apparent in one-dimensional ^{2}H MAS spectra may be larger than the pure dipole-dipole term. To exclude second-order contributions to the lineshape, the ^{2}H MAS spectrum should be compared with that recorded with a ^{15}N labelled sample. For both systems, contributions to R_{1Z} relaxation rate constants from spin-diffusion effects[56,57] are expected to be negligible if the chemical shift difference between the different ^{2}H sites is sufficiently large (≳ 3 ppm)[16,58,59] because the ^{2}H–^{2}H dipole-dipole "flip-flop" term cannot effectively couple two spin states with a significant energy separation.

In general, the spin-lattice relaxation of a resonance in a MAS spectrum will not be described by a single exponential decay because various crystallites that contribute to the observed signals may have different T_{1Z} values.[60] Nevertheless, the inversion recovery and the decay of the ^{2}H resonances at 10 kHz spinning frequency in L-histidine and oxalic acid appear to be well characterised by a single exponential. The trends of T_{1Z} and T_{1Q} across the spinning sideband manifolds as a function of temperature are shown in Figure 6a, c and Figure 7a, c, respectively. The T_{1Z} and T_{1Q} values averaged over the spinning sidebands are given in Table 3 and Table 4. In L-histidine, we note that the Zeeman relaxation time increases with temperature for δ-ND^+, ε-ND and D_2O, whereas it decreases as the temperature is increased for ND_3^+. The COOD and D_2O sites in oxalic acid show a trend similar to ND_3^+ in L-histidine, namely a decrease of the T_{1Z} as temperature is raised. At all temperatures, all ND_3^+ spinning sidebands relax with the same time constant, indicating little orientation dependence of T_{1Z} for motionally averaged deuterons. Torchia and Szabo[60] have shown for a methyl group diffusing freely in the extreme narrowing limit that the entire spectrum relaxes with the same T_{1Z}

Table 3. Zeeman spin-lattice relaxation times (T_{1Z}) averaged over all spinning sidebands as a function of temperature for each ^{2}H site in L-histidine hydrochloride monohydrate and α-oxalic acid dihydrate.

	L-Histidine hydrochloride monohydrate				α-Oxalic acid dihydrate	
T [K]	T_{1Z}(δ-ND^+) [s]	T_{1Z}(ε-ND) [s]	T_{1Z}(ND_3^+) [ms]	T_{1Z}(D_2O) [ms]	T_{1Z}(COOD) [ms]	T_{1Z}(D_2O) [ms]
268	0.59 ± 0.15	0.26 ± 0.10	16.2 ± 3	3.9 ± 1	258.6 ± 25.2	37.9 ± 15.8
288	0.71 ± 0.15	0.25 ± 0.07	11.8 ± 1	4.8 ± 0.3	–	–
298	0.83 ± 0.16	0.27 ± 0.07	9.1 ± 0.5	5.5 ± 0.1	43.6 ± 2.5	16.7 ± 0.8
308	0.93 ± 0.18	0.28 ± 0.07	6.9 ± 0.1	6.5 ± 0.1	26.4 ± 1.3	12 ± 0.5
318	1.02 ± 0.19	0.30 ± 0.06	5.6 ± 0.1	7.6 ± 0.1	–	–
328	1.16 ± 0.23	0.35 ± 0.07	4.7 ± 0.1	9.1 ± 0.3	11.5 ± 0.7	7 ± 0.3
338	1.18 ± 0.21	0.35 ± 0.07	4.2 ± 0.1	10.7 ± 0.3	8.3 ± 0.6	6 ± 0.3
358	1.25 ± 0.22	0.46 ± 0.09	3.7 ± 0.05	14.6 ± 0.7	–	–

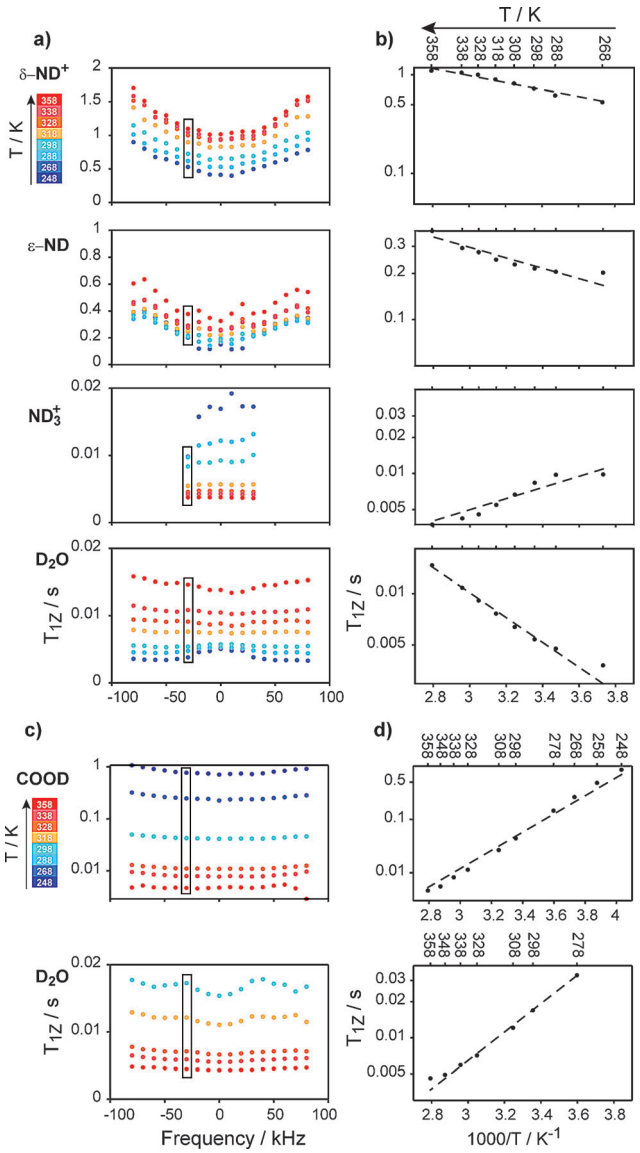

Figure 6. ^{2}H MAS T_{1Z} data as a function of temperature for each individual ^{2}H site in L-histidine hydrochloride monohydrate (a) and α-oxalic acid dihydrate (c). The T_{1Z} data are presented as an Arrhenius-type graph T_{1Z} vs. (1000/T) with a logarithmic scale for the ordinates, for the third left-side spinning sideband of each deuterium site (emphasised by boxes) together with corresponding fits (dashes) for L-histidine hydrochloride monohydrate (b) and α-oxalic acid dihydrate (d).

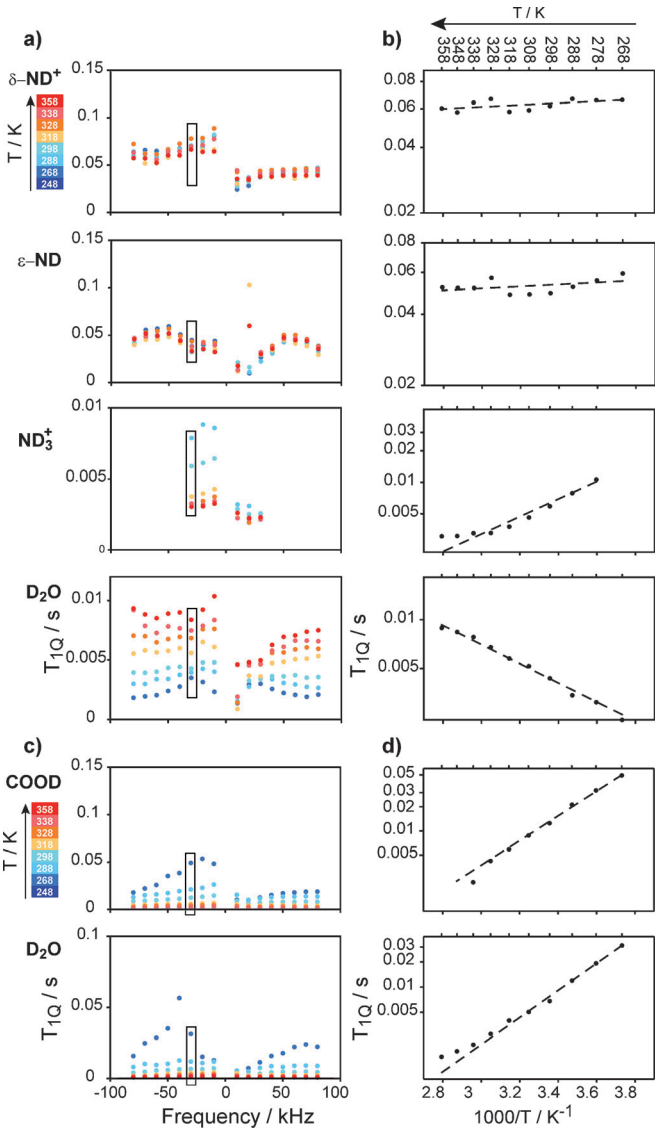

Figure 7. ^{2}H MAS T_{1Q} data as a function of temperature for each individual ^{2}H site in L-histidine hydrochloride monohydrate (a) and α-oxalic acid dihydrate (c). The T_{1Q} data are presented as Arrhenius-type graphs T_{1Q} vs. (1000/T) with a logarithmic scale of the ordinates for the third left-side spinning sideband of each deuterium site (emphasised by boxes) together with corresponding fits (dashes) for L-histidine hydrochloride monohydrate (b) and α-oxalic acid dihydrate (d).

relaxation time and that T_{1Z} becomes $27/(8C_Q^2\tau)$, where τ is the diffusion rate. Assuming the same geometry for ND_3^+ and assuming that we are in the extreme narrowing limit, the absence of any significant anisotropy of T_{1Z} indicates that the N–^{2}H bond diffuses freely about the C–N axis. Based on the previous relation, we can therefore estimate a correlation time of free diffusion between 0.2 ns at

Table 4. Quadrupolar order relaxation times (T_{1Q}) averaged over all spinning sidebands, except the centre band, as a function of temperature for each ^{2}H site in L-histidine hydrochloride monohydrate and α-oxalic acid dihydrate.

	L-Histidine hydrochloride monohydrate				α-Oxalic acid dihydrate	
T [K]	T_{1Q}(δ-ND^+) [ms]	T_{1Q}(ε-ND) [ms]	T_{1Q}(ND_3^+) [ms]	T_{1Q}(D_2O) [ms]	T_{1Q}(COOD) [ms]	T_{1Q}(D_2O) [ms]
268	57.4 ± 24	41.0 ± 13.4	13.7 ± 13.1	2.4 ± 0.6	30.9 ± 25.5	22.2 ± 12.7
288	56.5 ± 20.7	35.8 ± 11.8	6.2 ± 3.1	3.3 ± 0.7	18.0 ± 9.3	9.9 ± 3.6
298	56.5 ± 19.6	37.0 ± 9.5	4.8 ± 2.1	3.9 ± 0.8	10.6 ± 5.1	5.4 ± 2.1
308	50.1 ± 15.5	34.6 ± 10.0	3.9 ± 1.5	4.3 ± 1.0	7.7 ± 3.0	3.9 ± 1.5
318	51.7 ± 19.4	40.1 ± 18.6	3.4 ± 1.2	5.1 ± 1.3	5.4 ± 1.7	3.1 ± 1.2
328	61.4 ± 21.4	44.0 ± 11.0	3.0 ± 1.0	6.1 ± 1.5	3.8 ± 1.4	2.1 ± 0.9
338	56.8 ± 17.6	41.6 ± 10.6	2.9 ± 0.7	6.7 ± 1.8	2.5 ± 2.2	1.6 ± 0.6
358	50.8 ± 13.8	40.1 ± 11.3	2.8 ± 0.5	7.7 ± 1.8	–	1.1 ± 0.5

268 K and 1 ns at 358 K. Apperley et al.[61] analysed the ^{2}H T_{1Z} relaxation under MAS and remarked that the relaxation data were not very sensitive to the motional model. The relaxation rate of quadrupolar order, which is dominated by motions at the Larmor frequency, remains constant for the two ND sites of the imidazole ring in L-histidine, regardless of temperature. The motionally averaged ^{2}H sites in L-histidine and oxalic acid show the same behaviour as for Zeeman spin-lattice relaxation rates. Therefore, the T_{1Q} increased with temperature for D_2O in L-histidine and decreased as the temperature was increased for ND_3^+ in L-histidine, COOD and D_2O in oxalic acid. For none of the ^{2}H sites do either the Zeeman or the quadrupolar order relaxation time show a clear minimum over the temperature range investigated herein at a Larmor frequency of 61.4 MHz. Given that the absence of a well-defined minimum renders the interpretation of the relaxation data challenging, the activation energies derived from the T_{1Z} and T_{1Q} (Table 5) should be taken with caution.

The relaxation rate constants of SQ- and DQ-coherences can be further combined with the relaxation rate constants of the Zeeman and quadrupolar orders. The four relaxation rate constants measured at a given static magnetic field depend on the spectral density function evaluated at three distinct frequencies. Although of debatable applicability to solids, it is interesting to check the validity of the consistency relationship [Eq. (2)][17,32] originally derived for liquids in the fast motion limit (Redfield):

$$R_{DQ}^{fast} = \frac{1}{2}R_{1Z} + \frac{1}{6}R_{1Q} \quad (2)$$

If we assume that this relationship holds, we can calculate the relaxation rate constants for DQ-transitions induced by fast motions, R_{DQ}^{fast}, and compare them to the experimental values R_{DQ} measured at 61.4 MHz. This consistency test is only satisfied at near 328 K for ND_3^+ of L-histidine (data not shown). We ascribe the discrepancy between the calculated and measured R_{DQ} rates to the presence of additional slow motion processes (i.e. $R_{DQ} = R_{DQ}^{fast} + R_{DQ}^{slow}$). The relaxation rate constants for DQ-transitions induced by slow motions are given by Equation (3):

$$R_{DQ}^{slow} = R_{DQ} - R_{DQ}^{fast} \quad (3)$$

Indeed, the theoretical form of R_{DQ} in [Eq. (1d)] does not contain any dependence on slow motions because there are no contributions of $J_0(0)$. However, DQ coherence is subject to broadening by slow motions such as chemical exchange. For oxalic acid, slow motional processes, such as exchange between carboxyl and water protons, have been proposed to explain $T_{1Z}(^1H)$ relaxation times measured on a single crystal.[62] The graphs in Figure 8 a, b, e, f illustrate the relaxation rate constants of DQ coherences for fast motions, calculated from the R_{1Z} and R_{1Q} data by using the consistency relationship [Eq. (2)], and slow motions, obtained from the difference be-

Table 5. Averaged activation energy for individual ^{2}H sites in L-histidine hydrochloride monohydrate and α-oxalic acid dihydrate for T_{1Z} and T_{1Q} relaxation processes.

Molecule	^{2}H site	$E_a(T_{1Z})$ [kJ mol^{-1}]	$E_a(T_{1Q})$ [kJ mol^{-1}]
L-histidine	δ-ND^+	6.9 ± 0.6	0.5 ± 0.5
hydrochloride	ε-ND	6.5 ± 2.3	0.5 ± 0.5
monohydrate	ND_3^+	14.1 ± 2.4	12.2 ± 6.9
	D_2O	13.7 ± 1.4	10.7 ± 2.7
α-oxalic acid	COOD	32.6 ± 0.9	22.1 ± 5
dihydrate	D_2O	22.6 ± 2.7	27.6 ± 9.1

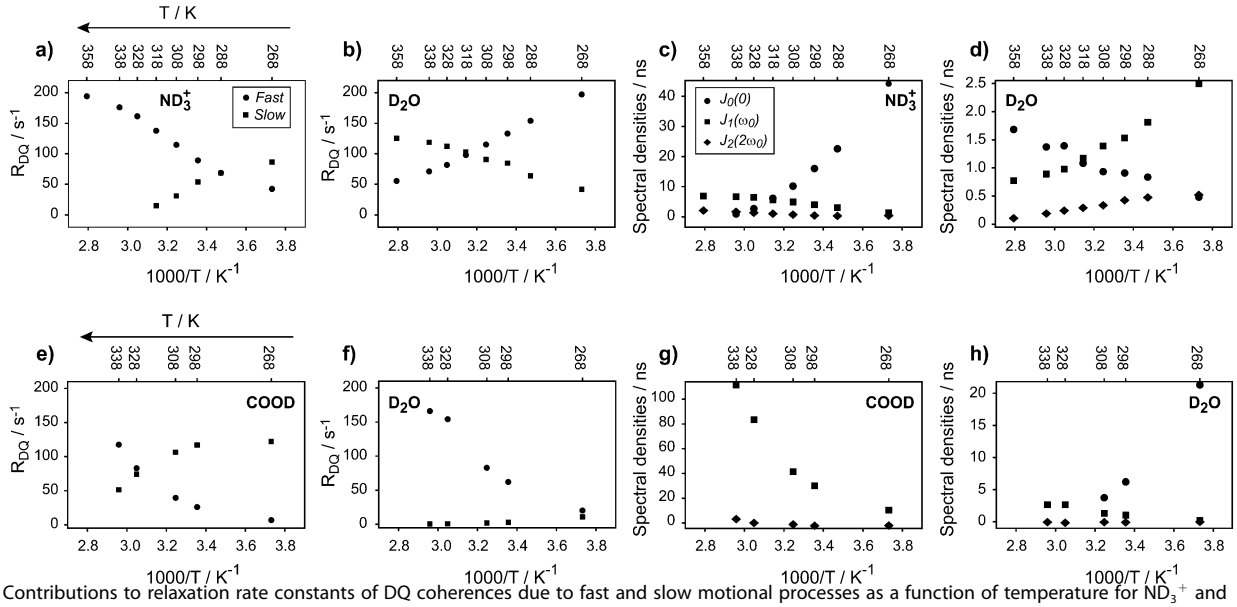

Figure 8. Contributions to relaxation rate constants of DQ coherences due to fast and slow motional processes as a function of temperature for ND_3^+ and D_2O in L-histidine hydrochloride monohydrate (a, b) and COOD and D_2O in α-oxalic acid dihydrate (e, f). The relaxation rate constants have been calculated as explained in the text. When possible the $J_0(0)$, $J_1(\omega_0)$ and $J_2(2\omega_0)$ have been determined based on Equations (1a–d). They are displayed as a function of temperature in Panels (c, d) for ND_3^+ and D_2O in L-histidine hydrochloride monohydrate and in Panels (g, h) for COOD and D_2O in α-oxalic acid dihydrate. The legend for Panels a, b, e and f is shown in Panel a and the legend for c, d, g and h is displayed in Panel c.

tween the experimental R_{DQ} and R_{DQ}^{fast}. This implies, as expected, that the relaxation rate constants of fast and slow motions are additive.

4. Conclusions

We have measured the temperature dependence of the SQ and DQ linewidths in ^{2}H MAS SQ–DQ spectra and of the relaxation times of Zeeman and quadrupolar order in two hydrated compounds recrystallised from heavy water. Even though a well-defined minimum in the T_{1Z} or T_{1Q} values was not found over the temperature range explored, we attempted to extract the barrier height of the motional process for each deuterium site in the two compounds. Discrepancies between the DQ relaxation rates measured experimentally and the relaxation rates calculated in the fast motion limit of the Redfield approximation suggest the coexistence of fast and slow motions. Molecular dynamics simulations would be very helpful to better understand the variations of these motions as a function of temperature. Overall, our results show that ^{2}H MAS can provide valuable information on the structure and motion of systems containing deuterons in polycrystalline solids. Similar studies can yield insight into dynamics processes on catalytic surfaces, in proteins and in nucleic acids.

Acknowledgements

The authors thank Quentin Llopis for his contributions in the early stages of this work, Nicole Fauré and Smita Odedra for evaluating some Jeener–Broekaert experiments, Philippe Pelupessy, Daniel Abergel, Piotr Tekely, Christian Bonhomme, Joanna R. Long and Robert Graf for stimulating discussions. NMR spectroscopic calculations were performed at the IDRIS supercomputer centre of the CNRS (Project 091461). M. C.-H., G. B. and L. D. acknowledge financial support from the Centre National de la Recherche Scientifique (CNRS, France), the Agence Nationale pour la Recherche (ANR, France) (grant ANR-09-BLAN-0111) and the European Research Council (ERC). Financial support from the IR-RMN-THC FR3050 CNRS for conducting preliminary experiments is gratefully acknowledged.

Keywords: deuterium · magic-angle spinning · molecular dynamics · NMR spectroscopy · solid-state structures

[1] J. W. Emsley, J. C. Lindon, *NMR Spectroscopy Using Liquid Crystal Solvents*, Pergamon Press, London, **1975**.
[2] R. E. Wasylishen, B. A. Pettitt, J. S. Lewis, *Chem. Phys. Lett.* **1979**, *67*, 459 – 462.
[3] H. W. Spiess, *Chem. Rev.* **1991**, *91*, 1321 – 1338.
[4] S. Opella, *Encyclopedia of Nuclear Magnetic Resonance* (Eds.: D. M. Grant, R. K. Harris), Wiley, Chichester, **1996**.
[5] K. Beshah, R. G. Griffin, *J. Magn. Reson.* **1989**, *84*, 268 – 274.
[6] S. K. Sarkar, Y. Hiyama, C. H. Niu, P. E. Young, J. T. Gerig, D. A. Torchia, *Biochemistry* **1987**, *26*, 6793 – 6800.
[7] J. R. Long, B. Q. Sun, A. Bowen, R. G. Griffin, *J. Am. Chem. Soc.* **1994**, *116*, 11950 – 11956.
[8] J. H. Kristensen, G. L. Hoatson, R. L. Vold, *Solid State Nucl. Magn. Reson.* **1998**, *13*, 1 – 37.
[9] M. Hologne, *Solid State Nucl. Magn. Reson.* **2004**, *26*, 1 – 10.
[10] C. Gardiennet, P. Tekely, *J. Phys. Chem. B* **2002**, *106*, 8928 – 8936.
[11] W. O. Parker, J. Hobley, V. Malatesta, *J. Phys. Chem. A* **2002**, *106*, 4028 – 4031.
[12] Y. Paik, J. P. Osegovic, F. Wang, W. Bowden, C. P. Grey, *J. Am. Chem. Soc.* **2001**, *123*, 9367 – 9377.
[13] S. J. Varner, R. L. Vold, G. L. Hoatson, *J. Magn. Reson.* **2000**, *142*, 229 – 240.
[14] G. Facey, D. Gusev, R. H. Morris, S. Macholl, G. Buntkowsky, *Phys. Chem. Chem. Phys.* **2000**, *2*, 935 – 941.
[15] M. M. Maricq, J. S. Waugh, *J. Chem. Phys.* **1979**, *70*, 3300.
[16] M. Cutajar, M. H. Lewis, S. Wimperis, *Chem. Phys. Lett.* **2007**, *449*, 86 – 91.
[17] O. Millet, D. R. Muhandiram, N. R. Skrynnikov, L. E. Kay, *J. Am. Chem. Soc.* **2002**, *124*, 6439 – 6448.
[18] D. Sheppard, D.-W. Li, R. Brüschweiler, V. Tugarinov, *J. Am. Chem. Soc.* **2009**, *131*, 15853 – 15865.
[19] H. Fuess, D. Hohlwein, S. A. Mason, *Acta Crystallogr. Sect. B* **1977**, *33*, 654 – 659.
[20] T. M. Sabine, G. W. Cox, B. M. Craven, *Acta Crystallogr. Sect. B* **1969**, *25*, 2437 – 2441.
[21] A. Lehmann, P. Luger, C. W. Lehmann, R. M. Ibberson, *Acta Crystallogr. Sect. B* **1994**, *50*, 344.
[22] S. Wimperis, G. Bodenhausen, *Chem. Phys. Lett.* **1986**, *132*, 194 – 199.
[23] G. L. Hoatson, T. Y. Tse, R. L. Vold, *J. Magn. Reson.* **1992**, *98*, 342 – 361.
[24] S. Wimperis, *J. Magn. Reson.* **1990**, *86*, 46 – 59.
[25] C. J. Pickard, F. Mauri, *Phys. Rev. B* **2001**, *63*, 245101.
[26] P. Giannozzi, S. Baroni, N. Bonini, M. Calandra, R. Car, C. Cavazzoni, D. Ceresoli, G. L. Chiarotti, M. Cococcioni, I. Dabo, A. Dal Corso, S. de Gironcoli, S. Fabris, G. Fratesi, R. Gebauer, U. Gerstmann, C. Gougoussis, A. Kokalj, M. Lazzeri, L. Martin-Samos, N. Marzari, F. Mauri, R. Mazzarello, S. Paolini, A. Pasquarello, L. Paulatto, C. Sbraccia, S. Scandolo, G. Sclauzero, A. P. Seitsonen, A. Smogunov, P. Umari, R. M. Wentzcovitch, *J. Phys.: Condens. Matter* **2009**, *21*, 395502.
[27] J. P. Perdew, K. Burke, M. Ernzerhof, *Phys. Rev. Lett.* **1996**, *77*, 3865 – 3868.
[28] N. Troullier, J. L. Martins, *Phys. Rev. B* **1991**, *43*, 1993 – 2006.
[29] L. Kleinman, D. M. Bylander, *Phys. Rev. Lett.* **1982**, *48*, 1425.
[30] P. Pyykkö, *Mol. Phys.* **2008**, *106*, 1965 – 1974.
[31] A. G. Redfield, *IBM J. Res. Dev.* **1957**, *1*, 19 – 31.
[32] J. P. Jacobsen, H. K. Bildsøe, K. Schaumburg, *J. Magn. Reson.* **1976**, *23*, 153 – 164.
[33] H. W. Spiess, A. Steigel, *Dynamic NMR Spectroscopy*, Springer-Verlag, **1978**.
[34] P. Hodgkinson, L. Emsley, *J. Chem. Phys.* **1997**, *107*, 4808.
[35] T. Chiba, G. Soda, *Bull. Chem. Soc. Jpn.* **1971**, *44*, 1703 – 1704.
[36] A. Hoffmann, I. Schnell, *ChemPhysChem* **2004**, *5*, 966 – 974.
[37] T. Chiba, *J. Chem. Phys.* **1964**, *41*, 1352.
[38] J. Schmidt, D. Sebastiani, *J. Chem. Phys.* **2005**, *123*, 074501.
[39] G. Soda, T. Chiba, *J. Chem. Phys.* **1969**, *50*, 439.
[40] M. J. Hunt, A. L. Mackay, *J. Magn. Reson.* **1974**, *15*, 402 – 414.
[41] M. J. Hunt, A. L. Mackay, *J. Magn. Reson.* **1976**, *22*, 295 – 301.
[42] J. Schmidt, A. Hoffmann, H. W. Spiess, D. Sebastiani, *J. Phys. Chem. B* **2006**, *110*, 23204 – 23210.
[43] M. Hong, K. J. Fritzsching, J. K. Williams, *J. Am. Chem. Soc.* **2012**, *134*, 14753 – 14755.
[44] X.-J. Song, C. M. Rienstra, A. E. McDermott, *Magn. Reson. Chem.* **2001**, *39*, S30 – S36.
[45] X. Zhao, M. Eden, M. H. Levitt, *Chem. Phys. Lett.* **2001**, *342*, 353 – 361.
[46] P. Lorente, I. G. Shenderovich, N. S. Golubev, G. S. Denisov, G. Buntkowsky, H.-H. Limbach, *Magn. Reson. Chem.* **2001**, *39*, S18 – S29.
[47] M. J. Duer, C. Stourton, *J. Magn. Reson.* **1997**, *129*, 44 – 52.
[48] M. Cutajar, S. E. Ashbrook, S. Wimperis, *Chem. Phys. Lett.* **2006**, *423*, 276 – 281.
[49] N. H. M. Hogg, P. J. T. Boulton, V. E. Zorin, R. K. Harris, P. Hodgkinson, *Chem. Phys. Lett.* **2009**, *475*, 58 – 63.
[50] M. J. Thrippleton, M. Cutajar, S. Wimperis, *Chem. Phys. Lett.* **2008**, *452*, 233 – 238.
[51] J. Virlet, *Encyclopedia of Nuclear Magnetic Resonance*, Wiley, Chichester, **1996**.
[52] R. Eckman, L. Muller, A. Pines, *Chem. Phys. Lett.* **1980**, *74*, 376 – 378.
[53] T. Chiba, G. Soda, *Bull. Chem. Soc. Jpn.* **1968**, *41*, 1524 – 1532.

[54] A. Hoffmann, *Characterisation of Supramolecular Structures by Novel Recoupling Methods in Solid-State NMR*, Dissertation, Johannes Gutenberg Universität, Mainz, **2005**.
[55] F. F. Iwasaki, H. Iwasaki, Y. Saito, *Acta Crystallogr.* **1967**, *23*, 64 – 70.
[56] M. Alla, R. Eckman, A. Pines, *Chem. Phys. Lett.* **1980**, *71*, 148 – 151.
[57] W. Schajor, N. Pislewski, H. Zimmermann, U. Haeberlen, *Chem. Phys. Lett.* **1980**, *76*, 409 – 412.
[58] Z. Gan, P. Robyr, *Mol. Phys.* **1998**, *95*, 1143 – 1152.
[59] B. Reif, Y. Xue, V. Agarwal, M. S. Pavlova, M. Hologne, A. Diehl, Y. E. Ryabov, N. R. Skrynnikov, *J. Am. Chem. Soc.* **2006**, *128*, 12354 – 12355.
[60] D. Torchia, A. Szabo, *J. Magn. Reson.* **1982**, *49*, 107 – 121.
[61] D. C. Apperley, A. F. Markwell, I. Frantsuzov, A. J. Ilott, R. K. Harris, P. Hodgkinson, *Phys. Chem. Chem. Phys.* **2013**, *15*, 6422.
[62] T. Chiba, *Bull. Chem. Soc. Jpn.* **1979**, *52*, 3229 – 3235.

Received: July 25, 2014
Published online on October 30, 2014